JOURNAL OF APPLIED PHYSICS **101**, 033114 (2007)

Theoretical study of quantum well infrared photodetectors with asymmetric well and barrier structures for broadband photodetection

W. Liu, D. H. Zhang,[a] Z. M. Huang, and W. J. Fan
School of Electrical and Electronic Engineering, Nanyang Technological University, Singapore 639798, Singapore

(Received 14 August 2006; accepted 5 December 2006; published online 8 February 2007)

The n-type InGaAs/Al$_x$Ga$_{1-x}$As quantum well infrared photodetector (QWIP) with asymmetric graded barriers for broadband detection has been investigated theoretically based on the eight-band $\mathbf{k}\cdot\mathbf{p}$ model. It is found that the intersubband transitions from the ground state to all bound and continuum excited states contribute to the overall absorption and the bound-to-continuum (B-to-C) transitions dominate. The superposition of the bound-to-bound and B-to-C transitions results in a broad detection bandwidth, and both the detected wavelength and bandwidth can be tuned by the applied voltage. The analysis method is also applicable to the GaAs/In$_x$Ga$_{1-x}$As/In$_y$Ga$_{1-y}$As QWIP with step quantum wells. The calculated results are consistent with the reported experimental observations. © *2007 American Institute of Physics*. [DOI: 10.1063/1.2434938]

I. INTRODUCTION

The mature III-V compound growth and process technologies with high uniformity and excellent reproducibility have led to rapid developments in quantum well infrared photodefector (QWIP) devices.[1–4] The ability to accurately control the band structure and the spectral response promotes the studies of QWIPs for various advanced applications. In addition to the conventional single-color QWIPs with narrow response bandwidths, multicolor and broadband QWIPs employing complex quantum well (QW) structures have also emerged in recent years.[2,5–10] Duboz *et al.* have studied the effect of asymmetric barriers on the performance of GaAs/AlGaAs QWIPs experimentally.[7] Jiang *et al.* have reported a high-performance three-stack, three-color InGaAs/AlGaAs QWIP for the mid, long, and very long wavelength infrared detections.[2] Lee *et al.* have demonstrated multicolor, broadband QWIPs with multistack QWs, digital graded superlattice barriers, and linear-graded barriers systematically.[9] Touse *et al.* have reported near- and mid-infrared detections using GaAs/In$_x$Ga$_{1-x}$As/In$_y$Ga$_{1-y}$As step QWs recently.[10] A lot of theoretical work have been done to study the physics of intersubband transitions[11–16] and the electron transport in QWIPs.[17–19] Recently, Jovanović *et al.* have proposed a fully quantum mechanical model to estimate current density, responsivity, capture probability, etc.[20] For the intersubband transitions in the QWIPs with asymmetric structures, some theoretical studies have been done based on the single band model which cannot include the coupling effect of the conduction and valence bands.[9,21–23]

In this article, the intersubband transitions in QWIPs with asymmetric well and barrier structures are analyzed using an eight-band $\mathbf{k}\cdot\mathbf{p}$ model combined with the envelope-function Fourier expansion. Both the bound-to-bound (B-to-B) and bound-to-continuum (B-to-C) transitions are discussed in detail. The InGaAs/Al$_x$Ga$_{1-x}$As QWIP with linear-graded barriers (LGBs) for broadband detection and the GaAs/In$_x$Ga$_{1-x}$As/In$_y$Ga$_{1-y}$As QWIP with step QWs are chosen for our study.

II. THEORETICAL METHOD

The total wave function in the eight-band scheme which takes the conduction band, the heavy hole, light hole, and spin-orbit split-off bands into consideration can be expressed as

$$\Psi(r) = \sum_{j=1}^{8} F_j(r)u_j(r) = \sum_{j=1}^{8} \exp(ik_t\rho)\varphi_j(z)u_j(r), \tag{1}$$

where $F_j(r)$ is the envelope function, $u_j(r)$ is the periodic part of the Bloch basis functions at the zone center, $k_t=(k_x,k_y)$ is the two-dimensional in-plane wave vector, and $\rho=(x,y)$ is the two-dimensional in-plane space vector. The Bloch basis functions we used are listed below:

$$\begin{aligned}
u_1 &= |1/2,1/2\rangle_c = |S\uparrow\rangle,\\
u_2 &= |1/2,-1/2\rangle_c = |S\downarrow\rangle,\\
u_3 &= |3/2,3/2\rangle_v = -i\sqrt{1/2}|(X+iY)\uparrow\rangle,\\
u_4 &= |3/2,1/2\rangle_v = i\sqrt{2/3}|Z\uparrow\rangle - i\sqrt{1/6}|(X+iY)\downarrow\rangle,\\
u_5 &= |3/2,-1/2\rangle_v = i\sqrt{2/3}|Z\downarrow\rangle + i\sqrt{1/6}|(X-iY)\uparrow\rangle,\\
u_6 &= |3/2,-3/2\rangle_v = i\sqrt{1/2}|(X-iY)\downarrow\rangle,\\
u_7 &= |1/2,1/2\rangle_v = i\sqrt{1/3}|Z\uparrow\rangle + i\sqrt{1/3}|(X+iY)\downarrow\rangle,\\
u_8 &= |1/2,-1/2\rangle_v = -i\sqrt{1/3}|Z\downarrow\rangle + i\sqrt{1/3}|(X-iY)\uparrow\rangle,
\end{aligned} \tag{2}$$

where $|S\rangle$ denotes the s-like conduction band Bloch state and $|X\rangle$, $|Y\rangle$, and $|Z\rangle$ denote the p-like valence band Bloch states.

---

[a] Electronic mail: edhzhang@ntu.edu.sg

0021-8979/2007/101(3)/033114/7/$23.00

The envelope function $F_j(r)$ is then expanded to a discrete Fourier series[24–26] as follows:

$$F_j(r) = \exp[i(k_x x + k_y y)] \sum_m a_{j,m} \phi_m(z), \tag{3}$$

where

$$\phi_m(z) = \frac{1}{\sqrt{L}} \exp\left[i\left(k_z + m\frac{2\pi}{L} \right) z \right], \tag{4}$$

m is an integer denoting the order of related expansion term, k_z is the wave vector in the QW growth direction, and $L = L_W + L_B$ is the multiple quantum well (MQW) structure period, where L_W and L_B are the well and barrier widths, respectively.

Substituting Eq. (3) into the eight coupled differential equations of

$$\sum_{j'=1}^{8} [H_{j,j'} + U(z)\delta_{j,j'}] F_{j'}(r) = E F_j(r), \quad j = 1, \ldots, 8, \tag{5}$$

where $U(z)$ is the electronic potential function and $H_{j,j'}$ is the eight-band $\mathbf{k}\cdot\mathbf{p}$ Hamiltonian whose details are listed in the Appendix; then multiplying by $\phi_m^*(z)$ and integrating over L, one gets

$$\sum_{j',m'} H_{j,j'}(m,m') a_{j',m'} = E a_{j,m}, \quad j,j' = 1, \ldots, 8, \tag{6}$$

where the matrix elements $H_{j,j'}(m',m)$ are given by

$$\begin{aligned} H_{j,j'}(m,m') &= \int_{-L/2}^{L/2} \phi_m^*(z) [H_{j,j'} + \delta_{j,j'} U(z)] \phi_{m'}(z) dz \\ &= \langle \phi_m^*(z) | H_{j,j'} + \delta_{j,j'} U(z) | \phi_{m'}(z) \rangle. \end{aligned} \tag{7}$$

The electronic potential function $U(z)$ includes the QW potential from the band discontinuity between the well and barrier, the strain-induced potential adjustment, and the potential change by applied bias. The eigenenergies and eigenstates in the QWs can then be obtained by solving the giant algebraic set of coupled equations [Eq. (6)].

The following probability functions are introduced to determine the conduction band (CB), heavy hole (HH), light hole (LH), and spin-orbit split-off (SO) band components in each QW state:

$$\begin{aligned} P_n^{\mathrm{CB}} &= \sum_{j=1,2} \sum_m a_{n,j,m}^* a_{n,j,m}, \\ P_n^{\mathrm{HH}} &= \sum_{j=3,6} \sum_m a_{n,j,m}^* a_{n,j,m}, \\ P_n^{\mathrm{LH}} &= \sum_{j=4,5} \sum_m a_{n,j,m}^* a_{n,j,m}, \\ P_n^{\mathrm{SO}} &= \sum_{j=7,8} \sum_m a_{n,j,m}^* a_{n,j,m}, \end{aligned} \tag{8}$$

where n denotes the QW subband index. These probability functions are particularly useful in identifying the dominant character in a particular energy state. The following sum rule should hold:

$$\sum_i P_n^i = 1, \quad i = \mathrm{CB}, \mathrm{HH}, \mathrm{LH}, \mathrm{SO}. \tag{9}$$

The momentum matrix element between subbands n and n' is

$$M_{nn'} = \langle \Psi_n | e_v \cdot \mathbf{p} | \Psi_{n'} \rangle = \sum_{j,j'=1}^{8} \langle F_{n,j} u_j | e_v \cdot \mathbf{p} | F_{n',j'} u_{j'} \rangle, \tag{10}$$

where $\mathbf{p}$ is the momentum operator and $e_v = \nu_x e_x + \nu_y e_y + \nu_z e_z$ $(\nu_x^2 + \nu_y^2 + \nu_z^2 = 1)$ is the photon polarization unit vector. Substituting Eqs. (1) and (3) into (10), we obtain

$$\begin{aligned} M_{nn'} &= \sum_{j,j'=1}^{8} \left\langle \sum_m a_{n,j,m} \phi_m(z) u_j | e_v \cdot \mathbf{p} | \sum_{m'} a_{n',j',m'} \phi_{m'}(z) u_{j'} \right\rangle \\ &\approx \sum_{j,j'=1}^{8} \Bigg[\left\langle \sum_m a_{n,j,m} \phi_m(z) | e_v \cdot \mathbf{p} | \sum_{m'} a_{n',j',m'} \phi_{m'}(z) \right\rangle \\ &\quad \times \langle u_j | u_{j'} \rangle \Bigg] \\ &\quad + \sum_{j,j'=1}^{8} \Bigg[\left\langle \sum_m a_{n,j,m} \phi_m(z) | \sum_{m'} a_{n',j',m'} \phi_{m'}(z) \right\rangle \\ &\quad \times \langle u_j | e_v \cdot \mathbf{p} | u_{j'} \rangle \Bigg]. \end{aligned} \tag{11}$$

Since $\langle u_j | u_{j'} \rangle = \delta_{jj'}$ and $\langle \phi_m(z) | \phi_{m'}(z) \rangle = \delta_{mm'}$, Eq. (13) becomes

$$\begin{aligned} M_{nn'} &= \sum_{j=1}^{8} \left[\left\langle \sum_m a_{n,j,m} \phi_m(z) | e_v \cdot \mathbf{p} | \sum_{m'} a_{n',j,m'} \phi_{m'}(z) \right\rangle \right] \\ &\quad + \sum_{j,j'=1}^{8} \left[\sum_m (a_{n,j,m}^* \cdot a_{n',j',m}) \langle u_j | e_v \cdot \mathbf{p} | u_{j'} \rangle \right], \end{aligned} \tag{12}$$

where the first term on the right of Eq. (12) is the transitions within the same Bloch basis states (intraband contribution), and the second term is the transitions between $|S\rangle$ and $|v\rangle$ ($|v\rangle = |X\rangle$, $|Y\rangle$, or $|Z\rangle$) states (interband contribution). With $M_{nn'}$ the absorption coefficient between subbands n and n' can be calculated by

$$\begin{aligned} \alpha_{nn'}(\hbar\omega) &= \frac{\pi e^2}{n_r c \varepsilon_0 m_0^2 \omega} \frac{2}{V} \sum_{k_t} |M_{nn'}|^2 (f_n - f_{n'}) \\ &\quad \times (\Gamma/2\pi)/[(E_{n'} - E_n - \hbar\omega)^2 + (\Gamma/2)^2], \end{aligned} \tag{13}$$

where f_n and $f_{n'}$ are the Fermi-Dirac distributions for electrons in respective subbands, Γ is the Lorentzian linewidth for the scattering relaxation, k_t is the in-plane wave vector, e is the electron charge, ε_0 is the free-space dielectric constant, n_r is the refractive index, and ω is the photon frequency.[11]

III. STRUCTURES AND PARAMETERS

The structures to be analyzed are the InGaAs/$\mathrm{Al}_x\mathrm{Ga}_{1-x}\mathrm{As}$ QWIP with LGBs and the GaAs/$\mathrm{In}_x\mathrm{Ga}_{1-x}\mathrm{As}$/$\mathrm{In}_y\mathrm{Ga}_{1-y}\mathrm{As}$ QWIP with multiple step

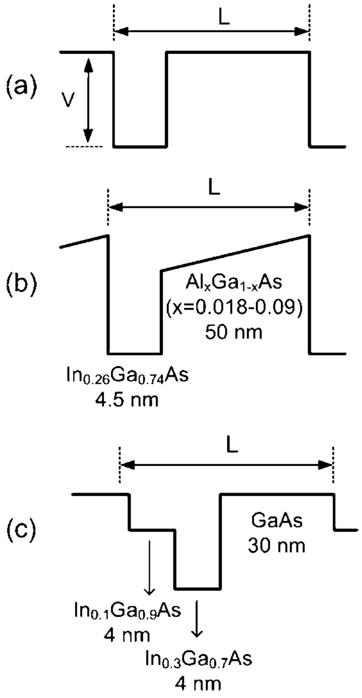

FIG. 1. Schematic conduction band profiles at zero bias of (a) symmetrical rectangular MQW, (b) $InGaAs/Al_xGa_{1-x}As$ LGB-QWIP, and (c) $GaAs/In_xGa_{1-x}As/In_yGa_{1-y}As$ QWIP with multiple step QWs. L is the MQW structure period.

QWs. The schematic conduction band diagrams of them are shown in Figs. 1(b) and 1(c), respectively. The $InGaAs/Al_xGa_{1-x}As$ MQW structure consists of 4.5 nm $In_{0.26}Ga_{0.74}As$ wells with a Si doping concentration of 7×10^{17} cm^{-3} and 50 nm $Al_xGa_{1-x}As$ barriers with the Al fraction x varying from 0.018 to 0.09. The $GaAs/In_xGa_{1-x}As/In_yGa_{1-y}As$ MQW sample consists of 4 nm $In_{0.3}Ga_{0.7}As$ wells with a Si concentration of 1×10^{18} cm^{-3}, 4 nm $In_{0.1}Ga_{0.9}As$ step wells, and 30 nm GaAs barriers. The overall dimensions from the top to the bottom contact layer are assumed to be 1.4 and 1.5 μm for the two QWIPs, respectively. The device structures enable us to directly compare our calculated results with the experimental observations reported in Refs. 9 and 10.

In the calculation the CB offset ratio between the $In_{0.26}Ga_{0.74}As$ well and the AlGaAs barrier is assumed to be 0.75.[27] The CB offset ratios between the $In_{0.3}Ga_{0.7}As$ and $In_{0.1}Ga_{0.9}As$ wells and the GaAs barrier are assumed to be 0.8 and 0.45, respectively.[28] Most parameters for the ternary compounds are obtained using a linear interpolation between the parameters of the relevant binary semiconductors listed in Table I except the band gap energy and electron effective mass. All the calculations are based on the material parameters for low temperature.

TABLE I. Parameters of binary compounds used in calculations (Ref. 29).

	GaAs	InAs	AlAs
Lattice constant a (Å)	5.6533	6.0584	5.6611
c_{11} (10 GPa)	12.21	8.329	12.50
c_{12} (10 GPa)	5.66	4.526	5.43
a_c (eV)	−7.17	−5.08	−5.64
a_v (eV)	1.16	1.0	2.47
b (eV)	−2.0	−1.8	−2.3
Luttinger parameter γ_1^L	6.98	20.0	3.76
Luttinger parameter γ_2^L	2.06	8.5	0.82
Luttinger parameter γ_3^L	2.93	9.2	1.42
Spin-orbit splitting energy Δ (eV)	0.341	0.390	280
Optical matrix parameter $E_P = 2P_0^2/m_0$ (eV)	28.8	21.5	21.1

IV. RESULTS AND DISCUSSIONS

Figure 2 shows the calculated energy dispersions of the conduction subbands $E1-E7$ as a function of the plane wave vector k_t along [100] and [110] directions of the $In_{0.26}Ga_{0.74}As/Al_xGa_{1-x}As$ (x=0.018−0.09) LGB-MQW under different positive biases. The InGaAs bulk valence band edge is taken as zero energy. The variations of subband dispersions with the wave vector in the QW growth direction (k_z) are considered in the calculation to account for the relaxation of quantum confinements for the excited states. As a consequence, the higher excited states appear to be minibands. Figure 3 shows the schematic conduction band profiles with subband levels at different applied biases. It can be seen that the excited states move downward gradually while

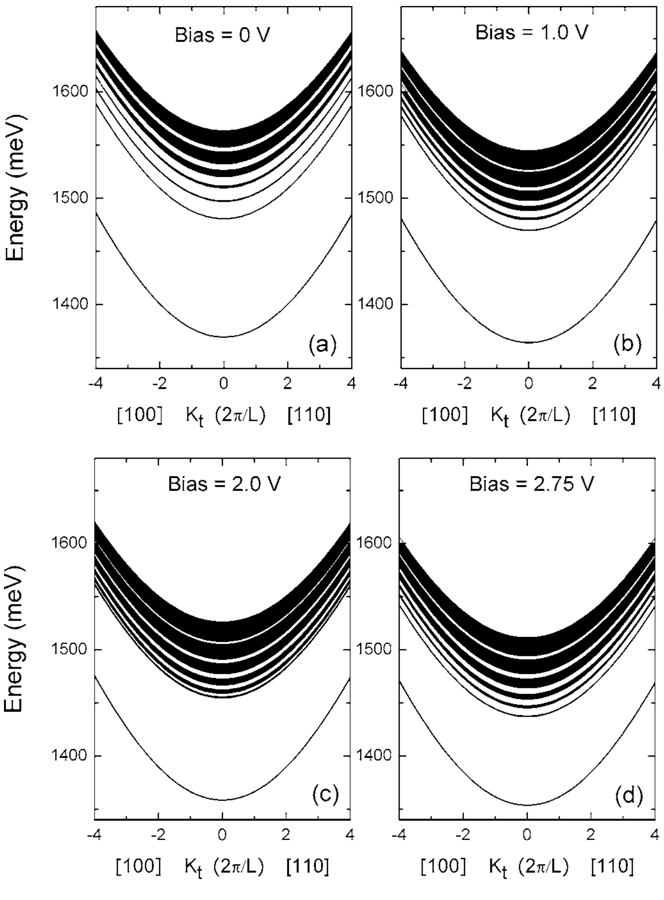

FIG. 2. The conduction subband energy dispersions of the $In_{0.26}Ga_{0.74}As/Al_xGa_{1-x}As$ (x=0.018−0.09) LGB-QWIP under different positive biases: (a) 0, (b) 1.0, (c) 2.0, and (d) 2.75 V.

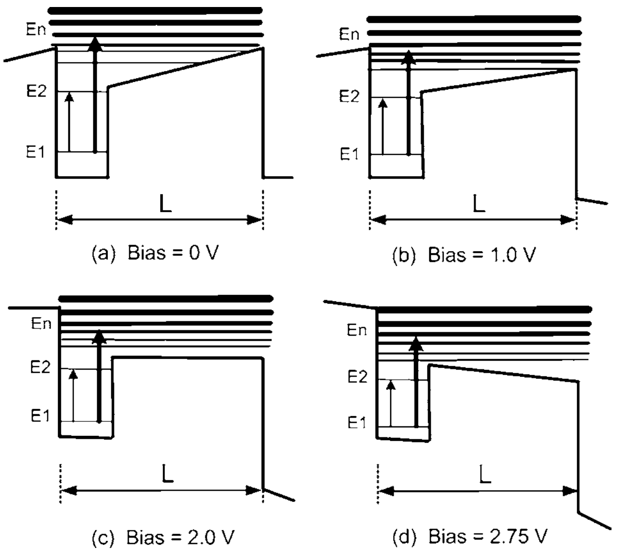

FIG. 3. A sketch of the conduction band profiles and subband levels of the InGaAs/Al$_x$Ga$_{1-x}$As LGB-QWIP for broadband detection at different positive biases.

the ground state remains relatively unchangeable with the reduction of the LGB height under increasing positive bias. As a result, the photoexcited electrons by the longer wavelength photons can easily transport through the barriers. At zero bias the lowest four subbands ($E1-E4$) are bound states. When 1.0 V bias is applied, the LGB is lowered and $E4$ becomes an unbound state. When the bias increases to 2.0 V or further, the LGBs are removed completely. Consequently, $E3$ also becomes unbound and the separations between the ground state $E1$ and the continuum excited states are decreased, resulting in the shifting of photodetection to longer wavelength.

The calculated squared optical transition matrix elements $Q_{\mathrm{TM},nn'}=2|M_{\mathrm{TM},nn'}|^2/m_0$ of $E1$ to different excited state transitions along the [110] k_t direction for normal to plane (TM) polarization under applied biases of 0 and 2.75 V are plotted in Fig. 4. The results for in-plane polarized (TE) transitions are not presented here since they are about three to four orders of magnitude smaller than the TM polarized ones. The transition matrix elements for a serial of k_z values between $m(2\pi/L)$ and $(m+1)(2\pi/L)$, where m is an integer, are computed, respectively, and are then integrated and normalized to obtain an overall outcome. This process is essential for calculating intersubband transitions involving continuum states. It is observed that all the transitions have significant intensities which are maximum at the zone center ($k_t=0$) and decrease slightly with increasing k_t. The $E1\rightarrow E4$, $E1\rightarrow E5$, and $E1\rightarrow E6$ transitions are stronger than the others.

The calculated optical absorption coefficient curves as a function of the optical wavelength for the LGB-QWIP at different positive biases are shown in Fig. 5. The linewidth Γ in Eq. (13) is assumed to be 16 meV in the calculation. At lower biases, i.e., 1.0 and 1.5 V, the absorption spectra in Figs. 5(a) and 5(b) peak at 10.0 and 10.8 μm, and the spectral full width at half maximum (FWHM) ranges are 7.9–12.6 and 8.2–12.8 μm, respectively. When the bias increases to 2.0 V, the spectral FWHM broadens to 5.2 μm (8.6–13.8 μm) with an absorption peak at 11.5 μm, as shown in Fig. 5(c). When the bias increases further to 2.75 V, the spectral FWHM increases to 7.0 μm (8.9–15.9 μm) with an absorption peak at 12.3 μm. The ratio of the FWHM to the peak wavelength ($\Delta\lambda/\lambda_p$) is about 56%, as shown in Fig. 5(d). The broad response spectrum is due to the superposition of comparable $E1\rightarrow E2-E8$ transitions. The $E1\rightarrow E4$, $E5$, and $E6$ transitions are relatively intensive. The calculation results clearly indicate that the detectable bandwidth broadens with increasing applied bias and expands to longer wavelength at the same time. The experimental data in Ref. 9 show that the peak of the photodetection spectrum shifted from 10.2 to12.0 μm and the spectral FWHM improved from about 4 to 6.3 μm when the bias applied on the LGB-QWIP was increased from 1 to 2.75 V. The calculated optical absorption coefficient curves are well consistent with the experimental observations.

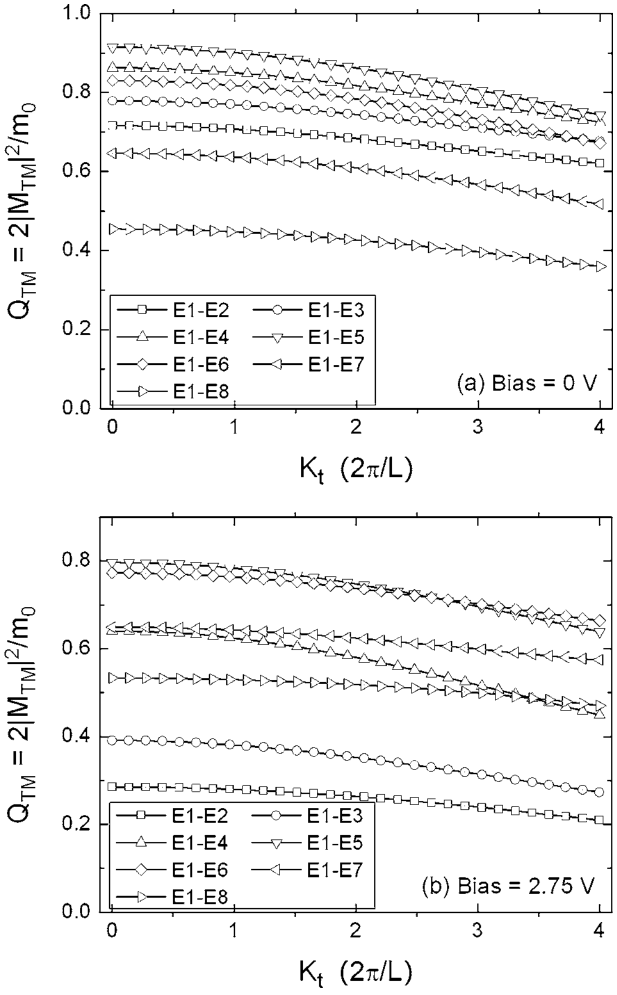

FIG. 4. Calculated squared optical transition matrix elements of TM polarization as a function of k_t for $E1$ to $E2-E8$ transitions in the LGB-QWIP under applied biases of (a) 0 and (b) 2.75 V, respectively.

It is found that the broken symmetry of the QW with the LGB structure changes the selectivity of intersubband transitions. This is a key reason for the broadband response. In ordinary symmetrical rectangular QWs, the B-to-B transition from the ground state to the bound first excited state is dominant while the B-to-C transitions are very weak.[1] The bias-

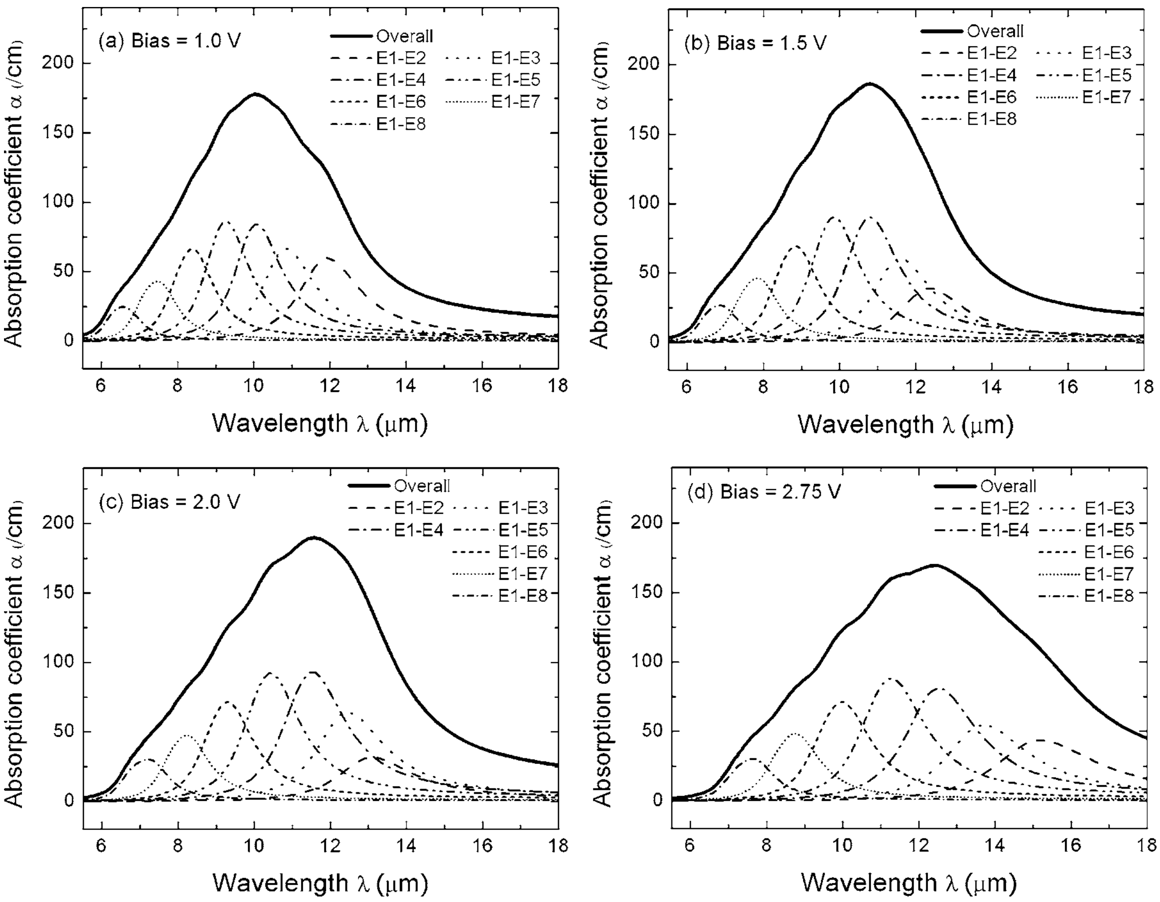

FIG. 5. Calculated intersubband optical absorption coefficients as a function of optical wavelength of the LGB-QWIP at different applied biases: (a) 1.0, (b) 1.5, (c) 2.0, and (d) 2.75 V.

dependent effects on the simple rectangular structures are relatively small because the symmetry only allows a quadratic electric-field shift. Consequently, the optical absorption spectrum is narrow usually. However, such rule becomes invalid in the asymmetric LGB-MQWs. All the B-to-B and B-to-C transitions of $E1 \rightarrow E2-E7$ have considerable rates and some B-to-C transitions are even stronger than the B-to-B $E1 \rightarrow E2$ transition. As a consequence, the superposition of all the transitions generates a very broad detection spectrum.

To further justify the validity of our eight-band method for asymmetric QWs, the theoretical analysis on the QWIP with $\mathrm{GaAs/In_{0.1}Ga_{0.9}As/In_{0.3}Ga_{0.7}As}$ multiple step QWs is done. The calculated subband energy dispersions versus k_t are plotted in Fig. 6 with the inset of schematic conduction band profile with the subband levels. The lowest five states in the conduction band ($E1-E5$) and in the valence band ($H1-H5$) are shown in the figure. The edge of bulk valence band of the $\mathrm{In_{0.3}Ga_{0.7}As}$ is taken as the position of zero energy. It is observed that the spin-up and spin-down states of the valence subbands split obviously at finite k_t due to the degeneration break resulting from the asymmetric structure. Actually this phenomenon also takes place in the conduction subband states, but the splitting is too small to be observed. It can be seen that the energy at the zone center of the ground state $E1$ is 1315.8 meV, which is below the $\mathrm{In_{0.1}Ga_{0.9}As}$ step well (bound states). The energy of $E2$ is 1429.0 meV which is very near the top of GaAs barrier (quasicontinuum state). The transition energies from the HH and LH ground states to $E1-E3$ are between 1282 and 1485 meV, corresponding to a wavelength range of 0.83–0.96 μm.

The calculated optical transition matrix elements and absorption coefficient spectra of different intersubband transitions at bias of 0.8 V are presented in Figs. 7 and 8, respectively. It is very interesting to find that the $E1 \rightarrow E3$ transition

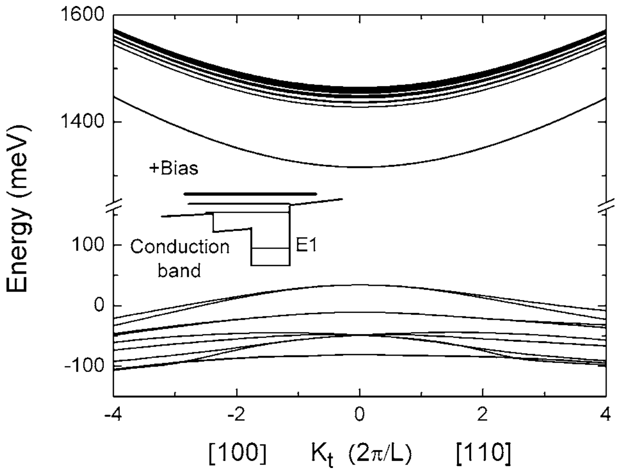

FIG. 6. The conduction subband energy dispersions of the $\mathrm{GaAs/In_{0.1}Ga_{0.9}As/In_{0.3}Ga_{0.7}As}$ QWIP at 0.8 V bias. The inset shows the schematic profile of conduction band of the step QW.

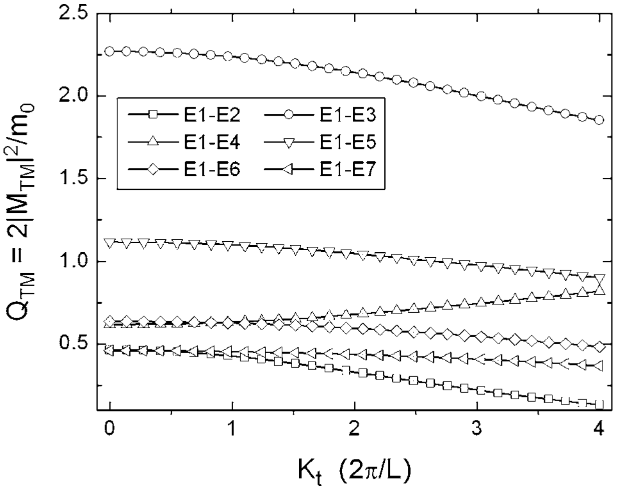

FIG. 7. Calculated squared optical transition matrix elements of TM polarization as a function of k_t of $E1$ to $E2-E7$ transitions for the GaAs/InGaAs QWIP with step QWs.

is dominant while the other transitions are relatively small. This unusual behavior results from the breaking of symmetry in the step QW structure, as what we have discussed for the LGB-QWIP in the last section. The intersubband transition selectivity for symmetrical rectangular QWs is not applicable for the step QW structure. The overall absorption spectrum peaking at 10.37 μm mainly comes from the $E1 \rightarrow E3$ transition. The experimental data in Ref. 11 of the multiple step QWs show near-infrared detection at 0.82–0.95 μm and mid-infrared detection with a peak at 10.4 μm, agreeing well with our theoretical results.

V. CONCLUSIONS

In conclusion, the eight-band $\mathbf{k}\cdot\mathbf{p}$ model is employed to study the intersubband transitions in the QWIP structures with asymmetric well and barrier structures. The results show that in the LGB-QWIPs, the B-to-B and B-to-C transitions studied all have considerable contribution, resulting in a very broad photodetection bandwidth. The detection peak shifts to longer wavelength gradually with the increasing bias and the detected bandwidth broadens. The B-to-C transitions dominate in all cases. Our calculated results are in good agreement with the reported experimental data.

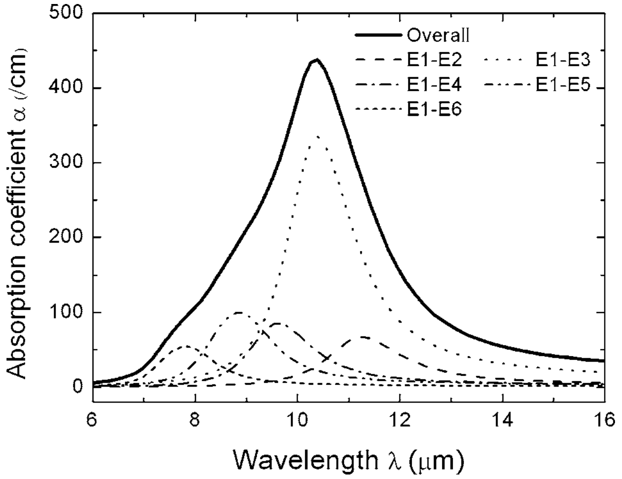

FIG. 8. Calculated intersubband optical absorption coefficients as a function of optical wavelength for the GaAs/InGaAs QWIP with step QWs.

ACKNOWLEDGMENTS

This work is supported by the Agency for Science, Technology, and Research, Singapore.

APPENDIX: EIGHT-BAND K·P HAMILTONIAN

The eight-band $\mathbf{k}\cdot\mathbf{p}$ Hamiltonian matrix $\mathbf{H}$ can be written with $\mathbf{H}=\mathbf{H}_k+\mathbf{H}_s$, where $\mathbf{H}_k$ is the basic $\mathbf{k}\cdot\mathbf{p}$ part and $\mathbf{H}_s$ is the strain part. $\mathbf{H}_k$ is given by

$$\mathbf{H}_k = \begin{bmatrix} C & 0 & -pk_+ & (\sqrt{2/3})pk_z & (1/\sqrt{3})pk_- & 0 & (1/\sqrt{3})pk_z & (\sqrt{2/3})pk_- \\ \cdots & C & 0 & (-1/\sqrt{3})pk_+ & (\sqrt{2/3})pk_z & pk_- & (\sqrt{2/3})pk_+ & (-1/\sqrt{3})pk_z \\ \cdots & \cdots & F & H & I & 0 & H/\sqrt{2} & \sqrt{2}I \\ \cdots & \cdots & \cdots & G & 0 & I & 1/\sqrt{2}(G-F) & -(\sqrt{3/2})H \\ \cdots & \cdots & \cdots & \cdots & G & -H & -(\sqrt{3/2})H^* & -1/\sqrt{2}(G-F) \\ \cdots & \cdots & \cdots & \cdots & \cdots & F & -\sqrt{2}I^* & H^*/\sqrt{2} \\ \cdots & \cdots & \cdots & \cdots & \cdots & \cdots & ((F+G)/2 \ -\Delta & 0 \\ \cdots & \cdots & \cdots & \cdots & \cdots & \cdots & \cdots & (F+G)/2-\Delta \end{bmatrix} \qquad \text{(A1)}$$

where

$$k_+ = (k_x + ik_y)/\sqrt{2}, \quad k_- = (k_x - ik_y)/\sqrt{2},$$

$$C = E_g + \frac{\hbar^2 k^2}{2m_0}\left[\frac{1}{m_e^*} - \frac{E_P}{3}\left(\frac{2}{E_g} + \frac{1}{E_g+\Delta}\right)\right],$$

$$F = Ak^2 + \frac{B}{2}(k^2 - 3k_z^2), \quad G = Ak^2 - \frac{B}{2}(k^2 - 3k_z^2), \qquad \text{(A2)}$$

$$H = -Dk_z(k_x - ik_y), \quad I = -\frac{\sqrt{3}}{2}B(k_x^2 - k_y^2) + iDk_xk_y,$$

$$A = -\frac{\hbar^2\gamma_1}{2m_0}, \quad B = -\frac{\hbar^2\gamma_2}{m_0}, \quad D = -\sqrt{3}\frac{\hbar^2\gamma_3}{m_0},$$

and

$$p = (\hbar/m_0)P_0,$$

where P_0 is the momentum matrix element for the conduction band, and γ_i $(i=1,2,3)$ are the modified Luttinger parameters[30] which are expressed as

$$\gamma_1 = \gamma_1^L - \frac{E_P}{3E_g}, \quad \gamma_2 = \gamma_2^L - \frac{1}{2}\frac{E_P}{3E_g}, \quad \text{and } \gamma_3 = \gamma_3^L - \frac{1}{2}\frac{E_P}{3E_g}, \tag{A3}$$

where γ_i^L $(i=1,2,3)$ are the usual Luttinger parameter, E_g is the material band gap, $E_P=2m_0p^2/\hbar^2$ is the optical matrix parameter, and m_e^* is the electron effective mass.

The strain Hamiltonian H_s can be derived by the following substitution because of the same underlying symmetry: $A \rightarrow a_v$, $B \rightarrow b$, $D \rightarrow d$, $k_\alpha k_\beta \rightarrow \varepsilon_{\alpha\beta}$ $(\alpha,\beta=x,y,z)$, and $\hbar^2k^2/2m_0 \leftrightarrow a_c$ for conduction band, where $\varepsilon_{\alpha\beta}$ is the strain tensor, b and d are the shear deformation potentials, a_v is the hydrostatic valence band deformation potential, and a_c is the conduction band deformation potential.

[1] B. F. Levine, J. Appl. Phys. **74**, R1 (1993).

[2] L. Jiang, S. S. Li, M. Z. Tidrow, W. R. Dyer, W. K. Liu, J. M. Fastenau, and T. R. Yurasits, Appl. Phys. Lett. **79**, 2982 (2001).

[3] H. C. Liu, C. Y. Song, A. J. Springthorpe, and J. C. Cao, Appl. Phys. Lett. **84**, 4068 (2004).

[4] M. Graf, G. Scalari, D. Hofstetter, J. Faist, H. Beere, E. Linfield, D. Ritchie, and G. Davies, Appl. Phys. Lett. **84**, 475 (2004).

[5] A. Majumdar, K. K. Choi, J. L. Reno, and D. C. Tsui, Appl. Phys. Lett. **83**, 5130 (2004).

[6] S. V. Bandara, S. D. Gunapala, J. K. Liu, S. B. Rafol, C. J. Hill, D. Z.-Y. Ting, J. M. Mumolo, and T. Q. Trinh, Appl. Phys. Lett. **86**, 151104 (2005).

[7] J. Y. Duboz, L. Saminadayar, and J. M. Gerard, J. Appl. Phys. **78**, 2803 (1995).

[8] X. Jiang, S. S. Li, and M. Z. Tidrow, IEEE J. Quantum Electron. **35**, 1685 (1999).

[9] J.-H. Lee, S. S. Li, M. Z. Tidrow, and W. K. Liu, Infrared Phys. Technol. **42**, 123 (2001).

[10] M. P. Touse, G. Karunasiri, K. R. Lantz, H. Li, and T. Mei, Appl. Phys. Lett. **86**, 093501 (2005).

[11] S. L. Chuang, in *Physics of Optoelectronic Devices*, Wiley Series in Pure and Applied Optics, edited by J. W. Goodman (Wiley, New York, 1995), Chap. 9.

[12] R. Q. Yang and J. M. Xu, Phys. Rev. B **50**, 7474 (1994).

[13] L. H. Peng and C. G. Fonstad, J. Appl. Phys. **77**, 747 (1995).

[14] J.-J. Shi and E. M. Goldys, IEEE Trans. Electron Devices **46**, 83 (1999).

[15] W. Shi, D. H. Zhang, and T. Osotchan, IEEE J. Quantum Electron. **36**, 835 (2000).

[16] C. W. Cheah, L. S. Tan, and G. Karunasiri, J. Appl. Phys. **91**, 5105 (2002).

[17] M. A. Gadir, P. Harrison, and R. A. Soref, Appl. Phys. Lett. **81**, 4272 (2002).

[18] V. Ryzhii, M. Ryzhii, and H. C. Liu, J. Appl. Phys. **92**, 207 (2002).

[19] O. O. Cellek and C. Besikci, Semicond. Sci. Technol. **19**, 183 (2004).

[20] V. D. Jovanović, P. Harrison, Z. Ikonić, and D. Indjin, J. Appl. Phys. **96**, 269 (2004).

[21] S. M. J. Okhovat-Alavian, A. Afzali-Kusha, and M. Kamarei, Proceedings of the 12th International Conference on Microelectronics, p. 181 (2000).

[22] E. Ozturk, H. Sari, and I. Sokmen, Solid State Commun. **132**, 497 (2004).

[23] J. M. Li, Y. W. Lub, X. X. Hana, J. J. Wua, X. L. Liua, Q. S. Zhua, and Z. G. Wang, Physica E (Amsterdam) **28**, 453 (2005).

[24] J.-B. Xia and W.-J. Fan, Phys. Rev. B **40**, 8508 (1989).

[25] D. Gershoni, C. H. Henry, and G. A. Baraff, IEEE J. Quantum Electron. **29**, 2433 (1993).

[26] S. T. Ng, W. J. Fan, Y. X. Dang, and S. F. Yoon, Phys. Rev. B **72**, 115341 (2005).

[27] D. J. Arent, Phys. Rev. B **41**, 9843 (1990).

[28] Z. Pan, L. H. Li, Y. W. Lin, B. Q. Sun, and D. S. Jiang, Appl. Phys. Lett. **78**, 2217 (2001).

[29] I. Vurgaftman, J. R. Meyer, and L. R. Ram-Mohan, J. Appl. Phys. **89**, 5815 (2001).

[30] K. Boujdaria, S. Ridene, and G. Fishman, Phys. Rev. B **63**, 235302 (2001).